



**HAL**  
open science

## Particle Image Velocimetry (PIV) measurements in a water film, application to a tire rolling through a puddle

D Cabut, M. Michard, V. Todoroff, J Lemaître, C. Hermange, Y. Le Chenadec, S Simoens

### ► To cite this version:

D Cabut, M. Michard, V. Todoroff, J Lemaître, C. Hermange, et al.. Particle Image Velocimetry (PIV) measurements in a water film, application to a tire rolling through a puddle. 24ème Congrès Français de Mécanique CFM 2019, Aug 2019, Brest, France. 10.1051/meca/2020052 . hal-02388865

**HAL Id: hal-02388865**

**<https://hal.science/hal-02388865>**

Submitted on 2 Dec 2019

**HAL** is a multi-disciplinary open access archive for the deposit and dissemination of scientific research documents, whether they are published or not. The documents may come from teaching and research institutions in France or abroad, or from public or private research centers.

L'archive ouverte pluridisciplinaire **HAL**, est destinée au dépôt et à la diffusion de documents scientifiques de niveau recherche, publiés ou non, émanant des établissements d'enseignement et de recherche français ou étrangers, des laboratoires publics ou privés.

# Particle Image Velocimetry (PIV) measurements in a water film, application to a tire rolling through a puddle.

D. Cabut<sup>a</sup>, M. Michard<sup>a</sup>, V. Todoroff<sup>b</sup>, J. Lemaître<sup>b</sup>, C. Hermange<sup>b</sup> Y. Le Chenadec<sup>b</sup>, S. Simoens<sup>a</sup>

a. Université de Lyon, Ecole Centrale de Lyon and LMFA UMR CNRS 5509, 36 Avenue Guy de Collongue, F-69134, Ecully, France, damien.cabut@ec-lyon.fr.

b. Manufacture Française des Pneumatiques Michelin, Clermont-Ferrand, France.

## Abstract :

*A measurement method based on Particle Image Velocimetry with refraction of the laser sheet at a window/water interface is proposed for the measurement of the velocity field of a water flow formed by a tire moving inside a water puddle. This study focuses on the feasibility and repeatability of this optical measurement method. The characterization of the optical properties of the measurement technique defines the integration effect in height of the measurement method. The analysis of the overall features of the flow is focused on two main zones in front and around the tire. The flow inside the first zone is defined by a characteristic velocity of the water displaced in an area located in front of the tire ; in the second zone a characteristic velocity representative of the flow in the vicinity of the shoulder of the tire is also defined. Correlations of both characteristic velocities with the car speed and water film height are established. New and worn tires were tested in this work.*

**Mots clefs : Free surface flow, Tire/road contact, multiphase flow, Particle Image Velocimetry.**

## Nomenclature :

**PIV** Particle image velocimetry.

**PMMA** Polymethyl methacrylate.

$V$  Vehicle speed.

$h_{water}$  Water height of the puddle.

$U$  Velocity of the fluid.

$U_x$  streamwise fluid velocity.

$U_x^{(b)}$  mean streamwise fluid velocity in the water bank.

$U_y$  spanwise fluid velocity.

$U_y^{(s)}$  maximum spanwise fluid velocity at the shoulder.

$I$  Pixel intensity on images.

$\theta_p$  Angle of the prism inclined face.

$n_w$  refractive index of water.

$n_p$  refractive index of PMMA.

$\delta t$  time step between laser pulses.

$\mu$  water dynamic viscosity.

$\rho$  water density.

$g$  gravity acceleration.

$\rho_p$  particles density.

$d_p$  particles diameter.

$V_p$  particles fall velocity.

$z_f$  falling distance of particles.

## 1 Introduction

The capacity of a tire to drain water is critical in order to avoid hydroplaning. This phenomenon happens when the water height and the vehicle speed are too high causing an accumulation of water in front of the tire. Due to this accumulation, the fluid exerts a lift force on the tire and then lifts the car up to the total loss of contact between the tire and the ground (Allbert 1968[3]). This causes a total loss of control of the vehicle. It has been demonstrated that current regulatory test (on vehicle wet braking from 20 to 80 km/h on 1 mm water depth) has some hydroplaning phenomenon when worn tires are used (Todoroff and al. 2018[13]). This is why the design of the grooves of a tire has to be optimized in order to evacuate enough water to avoid hydroplaning. To be more specific, if the drainage effect is not sufficient, the effect of the tire load on the water in front of the contact patch area induces a high hydrodynamic pressure in proportion to the square of the vehicle speed (Horne and al. 1963[5]).

Most experimental work related on hydroplaning are focused on the evolution of the contact patch area with different parameters as vehicle speed, water height or tire grooves geometry (Gengenbach 1968[6] and Horne and al. 1986[8]). The contact patch area identification is based on post-processing of images recorded with a camera below a window embedded on the road using fluorescent dye in the water puddle (J.Niskanen and al. 2014[11]). The evolution of the contact patch area with speed is important in order to quantify the uplift of the tire due to the hydrodynamic pressure and to classify tire grooves patterns with respect to their efficiencies. However, those measurements do not allow to quantify water flow rate in specific regions, like in the water bank or inside the grooves. Such flow rate quantification requires the quantitative knowledge of the velocity field in the liquid film near the contact patch.

The state of the art related to the velocity field structure in the vicinity of the contact patch for a car rolling through a puddle is mainly concerned with numerical studies (Hermange and al. 2017[7], Cho and al. 2006[4], Kumar and al. 2012[10] and Vincent and al. 2011[14]). On the other hand, to our knowledge, the literature related to velocity measurements is limited. Suzuki and Fukijama 2001[12] performed measurements using a technique derived from the so-called particle tracking technique. Velocity was determined by the trajectories of the tracer particles during the exposure time of the camera. Those

measurements provide an estimate of the water velocity in front of the tire but the lack of seeding particles in the measurement domain does not allow a full understanding of the flow. The precision of this method is also limited due to the uncertainty in the length of the particle trajectories for a single image with long exposure time ; moreover, measurements inside the grooves are not available.

In the present work, a different technique called PIV is used in order to estimate velocity of the fluid in front of the tire. PIV is an extensively used method in fluid mechanics in order to measure instantaneous velocity fields (Adrian and Yao 1985[1] and Adrian 1991[2]). For PIV measurements, seeding particles in the fluid are illuminated with a double pulsed laser light sheet. A pair of particle images is recorded with a double frame camera and processed using a cross correlation algorithm to determine the displacement of particle patterns in the flow. The time delay  $\delta t$  between laser pulses needs to be adjusted to the flow velocity range and the dimensions of the measurement area. This method has never been used for tire measurements mainly due to the lack of optical access, to a small signal/noise ratio and to the timing management which makes it difficult to apply PIV to a tire rolling through a puddle.

The measurement method and test facility are detailed in Sec.2. Optical parameters of the measurement method are described. Then the tire model and the different zones of study are presented. Thereafter, measurement results are given in Sec.3 and finally perspectives and conclusions are discussed in Sec.4.

## 2 Experimental facility and methods.

### 2.1 Facility and set-up

In this work, measurements are performed on a dedicated track at Michelin<sup>©</sup> Ladoux site (France). This track is composed of a straight road locally filled with a water film containing seeding particles as depicted Fig.1. The water height  $h_{water}$  is regulated between 2 and 8 mm with an ultrasound probe which controls the valves at the inlet and outlet of the puddle. A PMMA window of 500 mm thickness is embedded in the ground and allows an optical access from a room below the road. Due to the car rolling through the puddle and safety considerations, the laser emission optic cannot be placed at the ground level, neither in front of the tire, nor on the side of the water puddle. Therefore, seeding particles cannot be illuminated by a light sheet parallel to the ground as should be done for classical PIV measurements. The only available optical access is from the room located below the transparent window, using light refraction at the PMMA/water interface. In order to obtain a laser sheet propagating inside the water film with a low inclination angle, the window has a prismatic shape with a face inclined with an angle  $\theta_p = 66^\circ$ . This value of  $\theta_p$  is approximately the critical angle of total light reflection with respect to Snell-Descartes law :

$$\theta_t = a \sin \left( \frac{n_p}{n_w} \sin(\theta_i) \right) \quad (1)$$

$$T = 1 - R = 1 - \left| \frac{\tan \left( a \sin \left( \frac{n_p}{n_w} \sin(\theta_i) \right) - \theta_i \right)}{\tan \left( a \sin \left( \frac{n_p}{n_w} \sin(\theta_i) \right) + \theta_i \right)} \right|^2 \quad (2)$$

where  $n_p = 1.49$  is the refractive index of the PMMA incident medium,  $n_w = 1.33$  the refractive index of the water transmission medium,  $\theta_i$  is the incident ray angle before the interface,  $\theta_t$  is the transmitted ray angle,  $T$  is the transmission coefficient from the PMMA to the water and  $R$  is the reflection coefficient at the interface.

The orientation angle of the laser sheet optic has to be taken with a slight offset of approximately  $3^\circ$  compared to the normal of the inclined face of the prism to obtain enough transmission  $T$  of the light sheet to illuminate particles. Images of these particles are recorded with a camera placed below the prism (Fig.1)<sup>1</sup>.

## 2.2 Emitting and receiving optics characteristics

### 2.2.1 Emission

The laser sheet is generated by a double pulsed Laser :Yag (Litron Bernoulli) emitting at 532 nm. The light is generated using sheet optic composed of a spherical divergent lens in order to enlarge the laser beam before the convergent lens which minimize the thickness of the laser sheet at the beam waist and a cylindrical divergent lens to spread the laser beam in the spanwise horizontal direction. This light sheet optic is placed on a rotation stage to select the incident angle of the laser sheet on the prism. The precision on this angle is approximately  $0.1^\circ$ .

### 2.2.2 Seeding

With this refracted illumination method, the main problem is the noise induced by the spurious light trapped in the prism due to the part of the beam reflected at the interface which continues its propagation inside the PMMA. This noise can be reduced by the use of fluorescent particles. These particles emit light at a different wavelength than the illumination laser light. Therefore, by selecting the wavelength of the particles with the reception optic, spurious light can be reduced to ensure a good signal/noise ratio. The particles diameter is around  $20 - 50 \mu\text{m}$ . For an excitation at 532 nm the light emitted by fluorescence is around 584 nm.

### 2.2.3 Reception

Images of fluorescent particles are recorded with a double frame sCMOS camera whose sensor size is  $2155 \times 2560$  pixels (2560 in the streamwise direction and 2155 in the spanwise direction). An optical filter with a band-pass width of  $\pm 20$  nm centered at 590 nm is used for filtering all wavelengths out of interest. The efficiency of this filter is quantified by the transmission of 93% inside the band-pass filter and 3% outside the band-pass. The size of the measurement area is determined by the magnification factor (approximately  $M = 0.01$ ), depending on the lens and on the working distance between the lens and the water film. In this study, the focal distance of the lens is 100 mm and the working distance between the lens and the water film is around 1150 mm. The size of camera field of view is around  $205 \times 245$  mm (245 mm in the streamwise direction and 205 mm in the spanwise direction). The aperture number of the lens is 5.6.

The time between laser pulses depends on the vehicle speed according to Table.1. Interrogation areas of  $64 \times 64$  pixels with 75% overlap are used for the cross-correlation (which corresponds to a spatial resolution of  $6.125 \times 6.125$  mm).

---

1. This measurement method is patented (patent n° FR1900180).

## 2.3 Illumination and depth of focus

Particle tracking is based on the identification of individual particles, and becomes inefficient if particle density is too high. On the other hand, PIV measurements are based on the computation of cross-correlation between particles images in both frames of an image pair ; this cross-correlation is performed between elementary interrogation windows containing a set of seeding particles. The main parameter influencing the measurement of the cross-correlation function is the intensity of particle images on the camera sensor  $I_i$  (as expressed by R.J Adrian and al. 1991[2]) :

$$R_D = \sum_{x=0, y=0}^{x<n, y<n} I_1(x, y) \cdot I_2(x + dx, y + dy) \quad (3)$$

where  $R_D$  is the displacement component of the cross correlation function,  $x, y$  are the streamwise and spanwise coordinates inside the elementary interrogation window,  $n$  is the size of the interrogation window,  $(dx, dy)$  are the displacement components inside the interrogation window taken in the first and the second image and  $I_1$  and  $I_2$  are the intensities of the images 1 and 2 respectively.

For each interrogation area, the location  $(\delta x, \delta y)$  in the correlation plane of the peak value of  $R_D$  determines particle displacement components related to the most probable velocity of particles inside the interrogation window ; velocity components in this area are finally derived by dividing  $\delta x$  and  $\delta y$  by  $\delta t$ . The velocity measured with the PIV technique is then directly related to the intensity of particle images. This intensity is a combination of two optical parameters which are i) the illumination of the particles and ii) the position of fluorescent particles in the depth of focus of the camera. Therefore in order to identify particles in the water volume which contribute more in the velocity calculation, the depth of focus and the illumination function of the height of the particle in the puddle have to be determined.

Specific measurement methods are used in-situ when water is at rest to quantify the depth of field and the illumination profile in the height of the puddle. Firstly, the depth of focus is measured using a dotted matrix, composed of black dots of diameter 0.125 mm with a 0.250 mm space between them, on a white plate. The matrix is parallel to the window and fixed to a translation stage with a precision of 0.01 mm. Images of dots are recorded for a distance between ground and dotted matrix varying in the range 0.2 mm to 4 mm with a step of 0.2 mm (Fig.2).

The depth of focus is based on the analysis of dot gray levels. When dots are out of focus their apparent diameter increase while their gray levels decrease. Therefore, the inverse of dot intensity ( $1/I$ ) gives an information on the darkness of the dots and their quality of focus. This parameter is averaged on approximately 3500 dots on the matrix for each altitude of the matrix (Fig.3).

The depth of focus of the receiving optic is directly linked to the distance between the lens and the measurement zone (Kingslake 1992[9]). Therefore, measurements are made for the working distance used for PIV measurements (Fig.3). The evolution of the grey levels in the height of the puddle does not vary significantly in the whole water height. This shows that the focusing of particles is the same in all the puddle for the camera position and aperture used. Therefore, the focusing of particles does not influence the cross-correlation calculation.

For the light sheet intensity profile measurements, an inclined fluorescent plate (Fig.4) is placed in the puddle at different longitudinal positions in the measurement area. The fluorescent light emitted by the

inclined plate is recorded with the camera. The average intensity in the spanwise direction along the plate is then studied to know the light sheet intensity profile in the height of the puddle.

The inclined plate is then placed at 2 different  $x$  positions which are situated based on the coordinate system presented Fig.4 with the origin at the center of the contact patch in the spanwise direction and at the beginning of the contact patch in the streamwise direction. The measurement positions here are one position before the tire contact patch area (position 1 at  $x = -140$  mm) and one position at the beginning of the tire groove (position 2 at  $x = 12.5$  mm).

These measurements show that the intensity profile is almost uniform in the height for each  $x$  position in the measurement area (Fig.5). This result can be qualitatively explained as follows. The laser sheet emerging from the transparent window just after refraction is propagating inside the liquid film with an angle nearly equal to  $10^\circ$ . After some travel distance, the light sheet undergoes multiple reflections of the light sheet at the free surface and the intensity profile spreading is sufficient to produce a nearly uniform profile. Therefore, the illumination of particles is considered as homogeneous in the volume.

With those optical parameters, all particles in the puddle are illuminated with the same intensity and focused at each distance  $z$  from the ground. This is why all particles in the measurement volume contribute with the same weight to the cross-correlation algorithm. However, this cross-correlation function is a summation of all particles' contribution. Therefore, the particle density per unit of height is also important in the calculation.

## 2.4 Measurement protocol and Tire model

### 2.4.1 Fluorescent seeding particles

In order to minimize the intensity of optical noise introduced by the ambient light, measurements are made during the night. For all the following measurements and results, the inflation pressure of the tire is set to 2.2 bars. The origin of the reference frame is considered at the beginning of the contact patch in  $x$ , at the center of the contact patch in  $y$  (red star Fig.6) and at the floor in  $z$ . In this protocol, the seeding of the puddle is firstly made. Right after, the driver of the car initiates the car movement to the puddle. To control the speed of the car, the speed controller is activated. The time between the seeding of the puddle and the passage of the car is around 30 s. During this time, particles fall in the water puddle due to the gravity. In first approximation, a simplified equation of the particle falling in a steady puddle can be considered, taking into account the gravity, the buoyancy and the Stokes forces :

$$\begin{aligned} \frac{d\vec{V}_p}{dt} &= \frac{\rho_p - \rho}{\rho_p} \vec{g} - \frac{18\mu}{\rho_p d_p^2} \vec{V}_p \\ \Rightarrow V_p(t) &= -\tau_p \frac{\rho_p - \rho}{\rho_p} g \left[ 1 - e^{-t/\tau_p} \right] \end{aligned} \quad (4)$$

where  $\tau_p = \frac{\rho_p d_p^2}{18\mu}$  is the characteristic falling time.

With the time integration of the falling velocity, the distance traveled by a particle ( $z_f$ ) in the interval between the introduction of seeding particles and the car passage can be calculated. The distance traveled by the smallest particles ( $d_p = 20 \mu\text{m}$ ) during these 30 s is  $z_f = 1.2$  mm. The distance traveled by the largest particles ( $d_p = 50 \mu\text{m}$ ) during these 30 s is  $z_f = 7.8$  mm. Therefore, with this protocol,

even if the optical parameters does not select a preferential measurement height, the highest density of particles at the lowest altitudes induces an enhancement of the lowest height contribution to the cross-correlation. Therefore, the velocity measurements tend to be the velocity in the highest particle density zone (approximately between 0 and 4 mm height for a 8 mm puddle).

#### 2.4.2 Laser and camera synchronization

The natural working frequencies of both laser and camera are not high enough to perform time-resolved velocity measurements during a single car passage over the transparent window. Therefore, for each passage of the tire on the window, a single pair of images is recorded. For a given car speed  $V$  and water puddle height  $h_{eau}$ , the measurement is repeated over several passages. Synchronization between laser pulses and image recordings is performed using a commercial software (Davis8) combined with a programmable timing unit (PTU). An other timing to handle is the synchronization of the camera and the laser pulses with the passage of the car in the camera field of view. Several sensors are placed along the track to calculate with a real-time processor the actual velocity of the car ; the processor therefore computes the required time delay between the measurement time delivered by the last sensor and the arrival time of the tire in a specified area inside the camera field of view. A trigger signal generated by the processor is then sent to the PTU to start and synchronize the laser pulses with the particle image pair acquisition using the camera.

#### 2.4.3 Tire model and operating conditions

The objective of the present study is to focus on one tire model and to estimate the variability of velocity measurements for specific zones of interest of the flow in a puddle for a rolling tire. The tire chosen is a summer tire available on the market with dimension 225/45R17. This tire is composed of two main longitudinal grooves of section 12x7 mm (Type A), two thin longitudinal grooves (Type B) and transverse grooves (Type C) (Fig.6).

For this tire, two main zones of the flow are studied here for vehicle speeds ranging from  $V = 30$  km/h up to 80 km/h with a 10 km/h step. Typical velocity maps are presented in this paper for  $V = 50$  km/h. The first zone of interest is the flow in front of the tire in the part called "water bank". In this part the water is pushed along the tire rolling direction. The second part of the flow of interest is the flow at the shoulder in the spanwise direction ; which is the quantity of water that goes around the tire and which has no need to be drained by the grooves (Fig.7).

Two main tire configurations are tested. Firstly a new tire with 8 mm water height which corresponds to a water height slightly superior to the depth of the grooves of Type A. Finally a worn tire, buffed to the wear indicator, is tested with 2 mm water height which approximately corresponds to a 8 mm water height for a new tire.

### 3 Measurements and results

This paper is focused on some characteristic velocities derived zone by zone from PIV measurements. The objective is to study the evolution of these velocities with operating conditions, like car speed, water height or new/worn tires.

### 3.1 Variability of velocity measurements

A special procedure for velocity post processing, combining ensemble and/or spatial averaging is applied for two specific areas of interest in the vicinity of the contact patch. Different sources of flow variability from one snapshot to another can be identified.

However, for the same car speed and optics settlement, variability parameters can not be avoided between passages. The most noticeable source is the offset in the spanwise direction of the tire position over the window. The driver of the car can not always be perfectly aligned in the same position on the window. The standard deviation in the spanwise direction between passages (considering the different passages at every speed) is approximately 3 cm. This offset is random between passages and sometimes too large to keep the same part of the tire in the camera field. Therefore, it is difficult to superpose the different velocity fields in order to calculate the average velocity field (Fig.7).

An offset in the streamwise position of the tire is also possible. The speeds of the car are not exactly 30, 40, 50 km/h... The speed  $V$  of the car at the moment of the passages observes a standard deviation of approximately 1 km/h. This induced a small offset between passages of approximately 3 mm between passages. This offset has also to be considered in the flow analysis when the average velocity is calculated in different zones.

In order to avoid the appearance of spurious velocity vectors, the calculation of velocities is performed outside the contact patch zone defined by a geometric mask where no seeding particles are present. Due to the progressive particle density evolution near the contact patch, it's difficult to determine the exact zone where the contact patch begins. Therefore an uncertainty of approximately 3 mm can be assumed in the determination of the contact patch boundary which leads to some scatter in the water-bank and shoulder zone positions. All those variability sources induce many manual task requisitions in the velocity fields post-processing for the statistical analysis of the flow.

For the study of the variability of this measurement method, many passages are made at different car speeds for both new tire and worn tire respectively with  $h_{water} = 8$  mm and  $h_{water} = 2$  mm. All the passages studied in the present work are presented in Table.2.

### 3.2 Streamwise velocity in the water bank zone

The first zone of interest here is the water bank in front of the tire. In this area water is pushed in the streamwise direction. It corresponds to the water that is not evacuated by the tire, neither by drainage effect inside grooves nor by bypassing the tire at its shoulder. The two dimensional velocity field is presented in Fig.8 for a snapshot measured.

This velocity field shows that in front of the tire central rib, there is a zone of low velocity in the spanwise direction and with an almost uniform velocity in the streamwise direction. The spatial averaged velocity in the streamwise direction in the water bank zone (white rectangle Fig.8a)) is studied for different car speeds and for both configurations, with new tire with  $h_{water} = 8$  mm and with the worn tire with  $h_{water} = 2$  mm (Fig.9).

The dispersion of the points for the spatial averaged velocity in the water tank is low. That means that the streamwise velocity in this zone depends on the car speed. In order to study that dependence, the mean velocity is analyzed function of the car speed in Fig.10.

For both tire configurations, the velocity in the water bank ( $U_x^{(b)}$ ) seems to follow a linear evolution. This is why a linear regression is made in Fig.10. The linear regression for the new tires measurements

gives a coefficient of determination of  $R^2 = 0.9866$ . For the worn tire, the linear regression gives a coefficient of determination of  $R^2 = 0.9531$ . For the worn tire, the evolution of  $U_x^{(b)}$  function of  $V$  is less linear due to the lower  $R^2$ . The points from  $V = 30$  km/h to  $V = 60$  km/h are well approximated by the linear regression but at highest speeds ( $V = 80$  km/h) a small change of the behavior occurs and points are higher than the linear regression. To approximate this change of behavior, a quadratic interpolation is made Fig.10 for both configurations. For the new tire, the polynomial regression is close to the linear regression which is illustrated by the  $R^2 = 0.9874$  of the polynomial regression which is extremely close to the  $R^2$  of the linear regression. However, for the worn tire, the polynomial fit is a better approximation accounting for the high velocity points with a  $R^2 = 0.9874$  against  $R^2 = 0.9531$  for the linear regression.

In conclusion, the streamwise velocity in the water-bank generally follows a linear evolution for the new tire and the worn tire. For the worn tire an inflection point seems to appear for high vehicle speed contrary to the new tire. However, a lack of points at 80 km/h for the new tire makes it difficult to conclude on the behavior at high vehicle speed for this configuration.

### 3.3 Spanwise velocity at the shoulder.

The second zone of interest studied in this paper is the spanwise velocity at the shoulder. This zone corresponds to the water which bypass the tire at the shoulder. A major part of the evacuation of the water in front of the tire takes place in this part of the flow. The velocity fields are presented in Fig.11 for both streamwise and spanwise directions.

With these velocity fields, the flow at the shoulder of the tire shows a maximum velocity in the spanwise direction. In this particular shoulder zone, the velocity in the streamwise direction is low compared to the spanwise direction. The velocity along the line at the shoulder (black line Fig.11) is studied (Fig.12) in order to quantify the water evacuated by the side of the tire.

The same process have been repeated for different vehicle speeds on different measurement sessions and the spanwise velocity profile  $U_y^{(s)}$  along the black line Fig.11 remains the same. The velocity always growth linearly to a maximum of velocity and then falls down at the contact of the tire shoulder. The most pertinent parameter to quantify the amount of water bypassing the tire by the side appears to be the maximum of  $U_y$  on this line ( $U_y^{(s)}(V)$ ). This parameter is then studied for all vehicle passages for the new tire with  $h_{water} = 8$  mm and for the worn tire with  $h_{water} = 2$  mm (Fig.13).

The scatter of measurements is higher for  $U_y^{(s)}$  near the shoulder than the velocity  $U_x^{(b)}$  in the water bank. However, the reproducibility of the measurements remains relatively good. The spanwise velocity at the shoulder is therefore directly linked to the speed of the car. In order to study that dependence, this maximum velocity is analyzed as a function of the car speed in Fig.14.

As studied in the water bank, linear regression is made here. For the new tire, the linear regression gives a coefficient of determination of  $R^2 = 0.9348$ . For the worn tire, linear regression works well for points from 30 to 60 km/h but for high vehicle speed ( $V = 70$  km/h and  $V = 80$  km/h) the regression does not fit as seen for the water bank zone. Therefore, input parameters chosen for the linear regression are points from 30 to 60 km/h. The coefficient of determination of the linear regression is then  $R^2 = 0.8467$ . For the worn tire,  $U_y^{(s)}(V)$  as well as  $U_x^{(b)}(V)$  shows a change of regime around  $V = 60$  km/h where the linear regression is no more available. To approximate this change of behavior, a quadratic interpolation is made Fig.14 for both configurations. For the new tire, the polynomial regression is close to the linear regression with a similar coefficient of determination  $R^2 = 0.9357$ . However, for the worn tire, the

polynomial fitting is a better approximation of high speed points with a coefficient of determination  $R^2 = 0.9363$  which is significantly higher than the linear regression  $R^2 = 0.8467$ .

In conclusion, as previously shown for the water bank zone, the evolution of  $U_y^{(s)}(V)$  is generally linear with the speed for the new tire. For the worn tire, the evolution is linear until an inflection point where the regime change and can be approximated with a polynomial fitting. As previously mentioned, the lack of points at 80 km/h and beyond for the new tire does not allow to conclude on the presence or not of the change of regime for this configuration.

### 3.4 Hypothesis on the regime change

In those studies, it appears that both velocities (streamwise in the water bank and spanwise at the shoulder) evolve linearly as a function of the car speed depending on the tire wear and water height.

This linearity in the evolution of the speed for the velocity in the water bank  $U_x^{(b)}(V)$  can be explained by the fact that the water which is not drained is pushed by the tire in front of it. Also this linearity is interdependent between the different parts of the flow. In a first approximation, if a 2D flow in the tire referential is considered, the conservation of the mass flow rate in front of the tire gives a linear dependence between  $V$  and each variable  $U_x^{(b)}(V)$ ,  $U_y^{(s)}(V)$  and  $U_{grooves}$ , with  $U_{grooves}$  average draining velocity in the grooves. Therefore, a disturbance in the linear regime in one of these variables introduces a similar effect on other variables.

## 4 Summary and Conclusions

PIV using fluorescent particles is a measurement which allows the quantification of the velocity field in the water for a car rolling through a puddle. Despite variability of the method, the number of statistical samples allows to conclude on the convergence of the standard deviation of the measured velocities.

Two main areas of interest have been studied in order to characterize the flow in these regions. In both of them, the evolution of the velocity is directly related to the vehicle speed. This evolution can be considered as linear depending on the tire wear and water height. The streamwise velocity in the water bank and the spanwise velocity at the shoulder can be predicted with a linear regression until an inflection speed where a polynomial fit is used here. This inflection speed of the change of regime is approximately 60 km/h for the worn tire with  $h_{water} = 2$  mm and seems beyond 80 km/h for the new tire with  $h_{water} = 8$  mm (Fig.15). To know if the inflection point exists for the new tire and its position, new measurements have to be made to increase the number of points at  $V = 80$  km/h and to acquire points at 90 km/h.

To improve this velocity prediction parametric studies can be made in order to determine the coefficient of those regressions and the inflection velocity depending on the water height, the wear of the tire and the tire patterns dimensions.

The present measurement method also allows the classification of tires as a function of their hydroplaning sensitivity.  $U_x^{(b)}$  quantify the amount of water which is pushed streamwise and then not evacuated, neither by by-passing the tire at the shoulder, nor by draining in the grooves. Therefore, for the same vehicle speed  $V$ , a tire with higher  $U_x^{(b)}(V)$  stocks more water in the water bank and is more sensitive to the hydroplaning mechanism.

This study focused on 2 essential points to understand hydroplaning and shows good results on the study of the flow in front of a tire. However, the draining effect through the grooves was not investigated in

the present paper. The resolution used here is too low to allow the velocity field measurement in the tire grooves. Therefore, velocity measurements inside the grooves remains the most important challenge in order to characterize the flow either in grooves of A, B or C types. The potential presence of multiphase flow or eventually turbulence can be a key factor to understand the draining capacity of a tire function of the geometry of its grooves.

## Acknowledgment :

The authors would like to thank BPI France (grant n° DOS0051329/00) and Région Auvergne-Rhône-Alpes (grant n° 16 015011 01) for funding the Hydrosafe Tire FUI project.

## Références

- [1] Adrian, Ronald J and Yao, Chung-Sheng, Pulsed laser technique application to liquid and gaseous flows and the scattering power of seed materials, *Applied optics*, 24 (1985) 44–52.
- [2] Adrian, Ronald J, Particle-imaging techniques for experimental fluid mechanics, *Annual review of fluid mechanics*, 23 (1991) 261–304.
- [3] Allbert, BJ, Tires and Hydroplaning, *SAE Transactions*, (1968) 593–603.
- [4] Cho, JR and Lee, HW and Sohn, JS and Kim, GJ and Woo, JS, Numerical investigation of hydroplaning characteristics of three-dimensional patterned tire, *European Journal of Mechanics-A/Solids*, 25 (2006) 914–926.
- [5] Dreher, Robert C and Horne, WB Phenomena of pneumatic tire hydroplaning, *Procedia-Social and Behavioral Sciences*, (1963).
- [6] Gengenbach, W, Experimental investigation of tires on wet pavements, *Automotive technology magazine*, 70 (1968).
- [7] Hermange, C, Numerical simulation of the fluid-structure interactions inside the aquaplaning problem. Thèse, Ecole Centrale de Nantes, 2017.
- [8] Horne, Walter B and Yager, Thomas J and Ivey, Don L, Recent studies to investigate effects of tire footprint aspect ratio on dynamic hydroplaning speed, *The tire pavement interface*, (1986) ASTM International.
- [9] Kingslake, Rudolf, *Optics in photography*, 3 (1992).
- [10] Kumar, Srirangam Santosh and Anupam, Kumar and Scarpas, Tom and Kasbergen, Cor, Study of hydroplaning risk on rolling and sliding passenger car, *Procedia-Social and Behavioral Sciences*, 53 (2012) 1019–1027.
- [11] Niskanen, Arto J and Tuononen, Ari J, Three 3-axis accelerometers fixed inside the tyre for studying contact patch deformations in wet conditions, *Vehicle System Dynamics*, 52 (2014) 287–298.
- [12] Suzuki, Tadashi and Fujikawa, Tatsuo, Improvement of hydroplaning performance based on water flow around tires, *SAE Technical Paper*, (2001).
- [13] Todoroff, Violaine and Paupy, Sébastien and Biesse, Frederic and Le Chenadec, Yohan, The mechanisms involved during the wet braking of new and worn tires, *Vehicle System Dynamics*, (2018) 1–20.

- [14] Vincent, Stéphane and Sarthou, Arthur and Caltagirone, Jean-Paul and Sonilhac, Fabien and Février, Pierre and Mignot, Christian and Pianet, Grégoire, Augmented Lagrangian and penalty methods for the simulation of two-phase flows interacting with moving solids. Application to hydroplaning flows interacting with real tire tread patterns, *Journal of Computational Physics*, 230 (2011) 956–983.

**Tables :**

Vehicle speed $V$ (km/h)	30	40	50	60	70	80
Time step $\delta t$ ( $\mu s$ )	330	225	180	150	130	115

TABLE 1 – Time delay between laser pulses.

Tire type	30 km/h	40 km/h	50 km/h	60 km/h	70 km/h	80 km/h
New tire	20	8	16	20	16	2
Worn tire	16	8	12	8	8	8

TABLE 2 – Number of statistical samples for ensemble averaging.

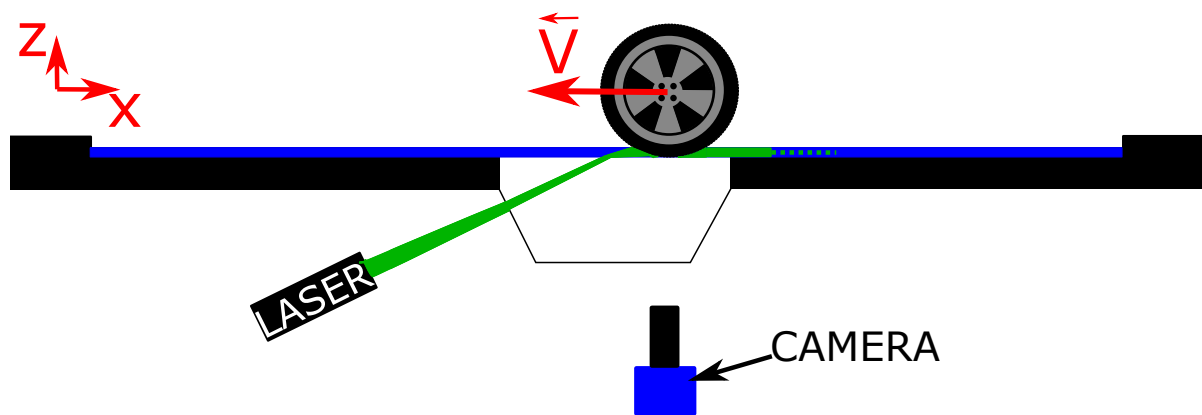
**Figures :**

FIGURE 1 – Scheme of the illumination method.

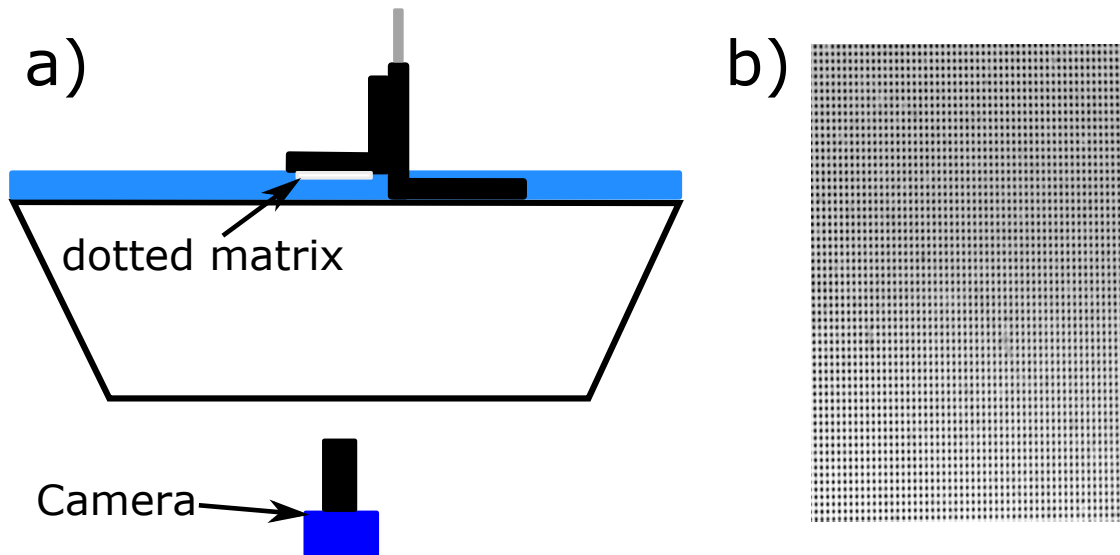


FIGURE 2 – a) Scheme of the dotted matrix on the translation stage in the puddle with the camera below the PMMA block. b) Image of the dotted matrix.

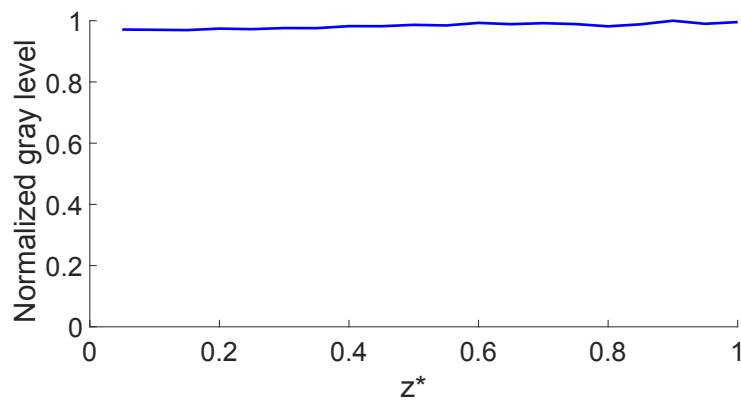


FIGURE 3 – Averaged gray level of dots function of the normalized height ( $z^* = z/h_{water}$ ) for a working distance of 1150 mm between the camera and the PMMA block.

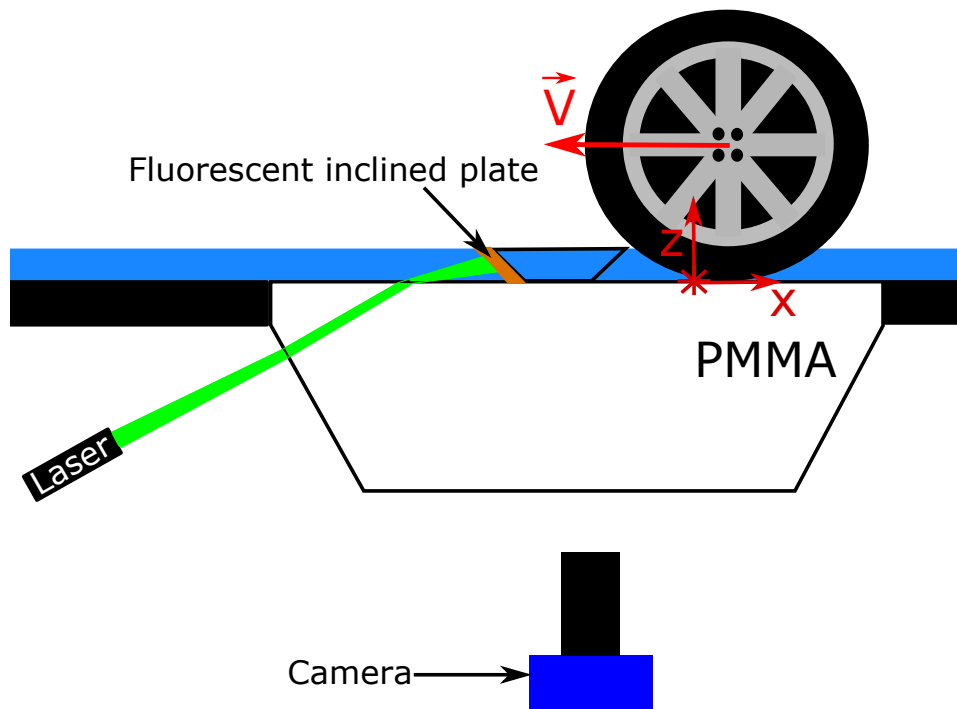


FIGURE 4 – Scheme of the inclined plane in the puddle. Red star corresponds to the origin of the referential at the beginning of the tire/road contact patch.

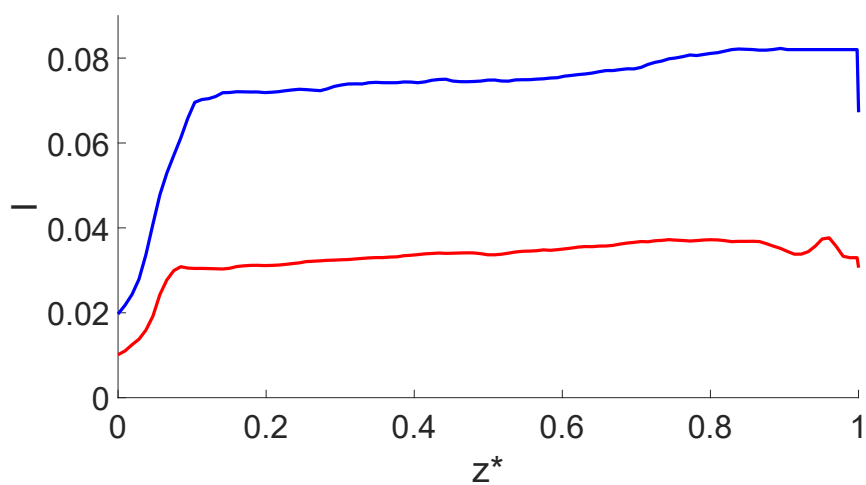


FIGURE 5 – Intensity function of the normalized height in the puddle ( $z^* = z/h_{water}$ ), blue for the position 1 and red for the position 2.

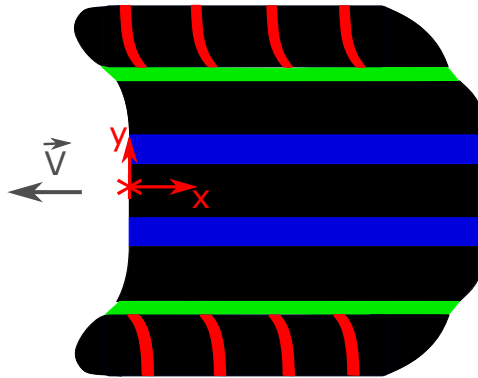


FIGURE 6 – Scheme of the contact patch of a PCY4 tire. Red are the Type C grooves, green are the Type B grooves and blue are the type A grooves.

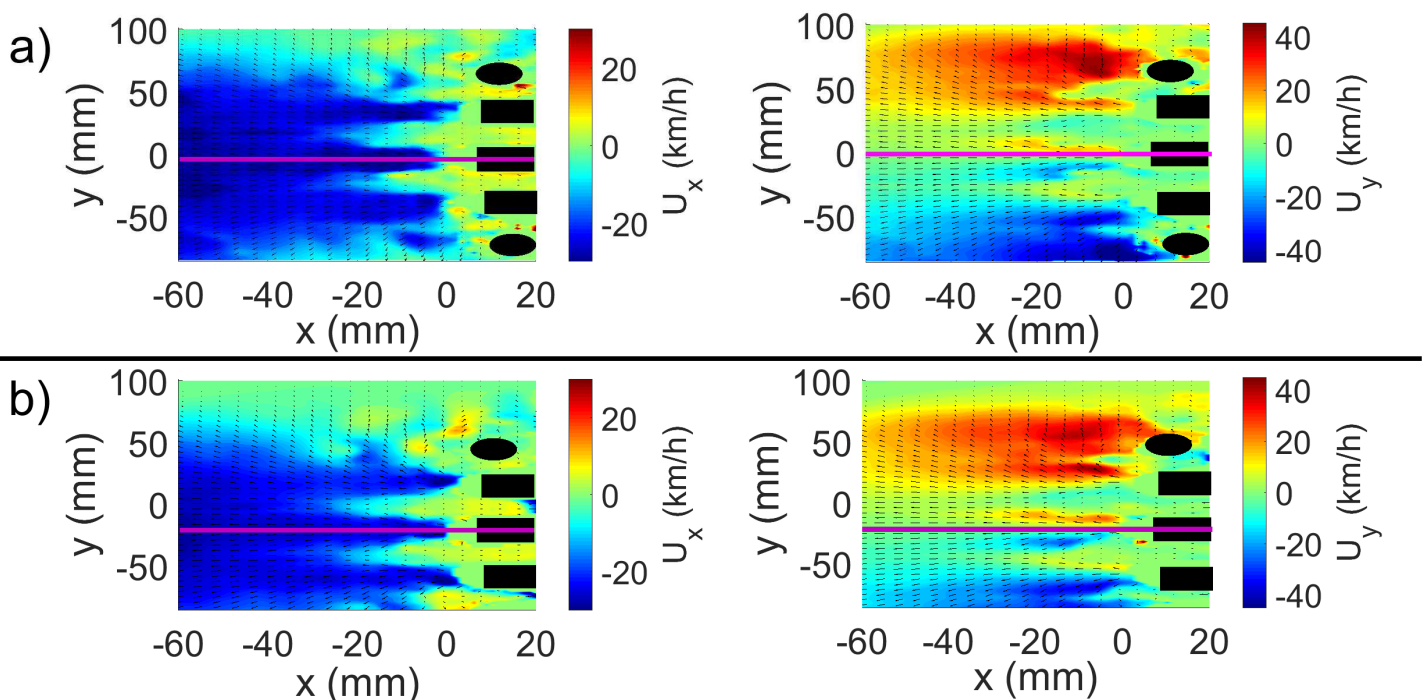


FIGURE 7 – Velocity field in the streamwise direction (Left) and spanwise direction (Right) for two consecutive passages of the car at  $V = 50$  km/h (a) passage 1 and b) passage 2). Black area is a scheme of the contact patch zone on these velocity field and the purple line symbolize the tire axis.

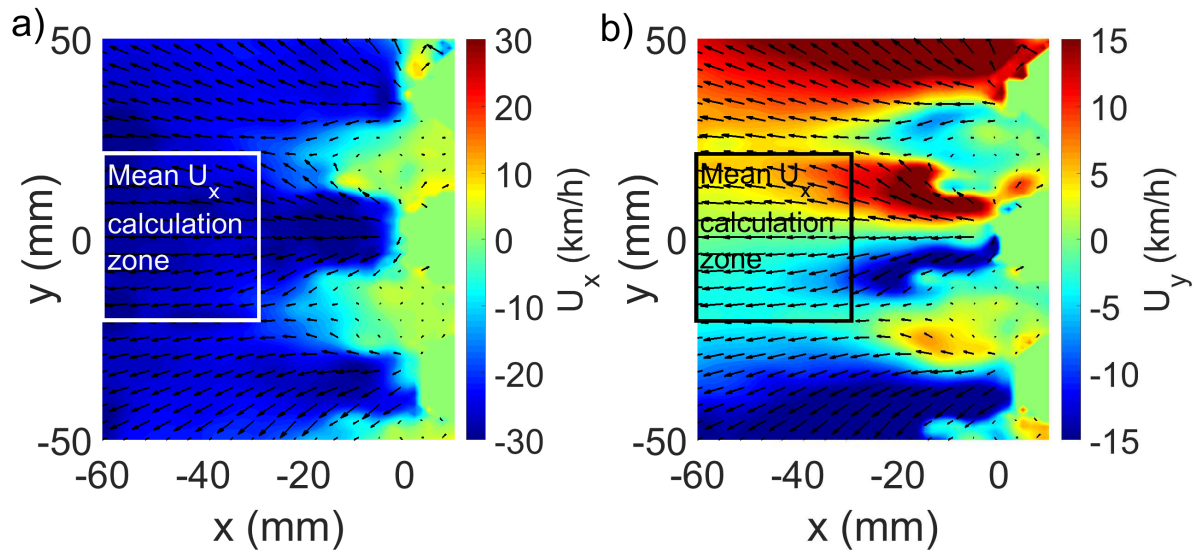


FIGURE 8 – Vector field in the front zone of the tire with colormap : a) streamwise velocity ( $U_x$ ), b) spanwise velocity ( $U_y$ ). For a new PCY4 tire rolling at 50 km/h with  $h_{water} = 8$  mm. Rectangles define the area of interest for spatial averaging.

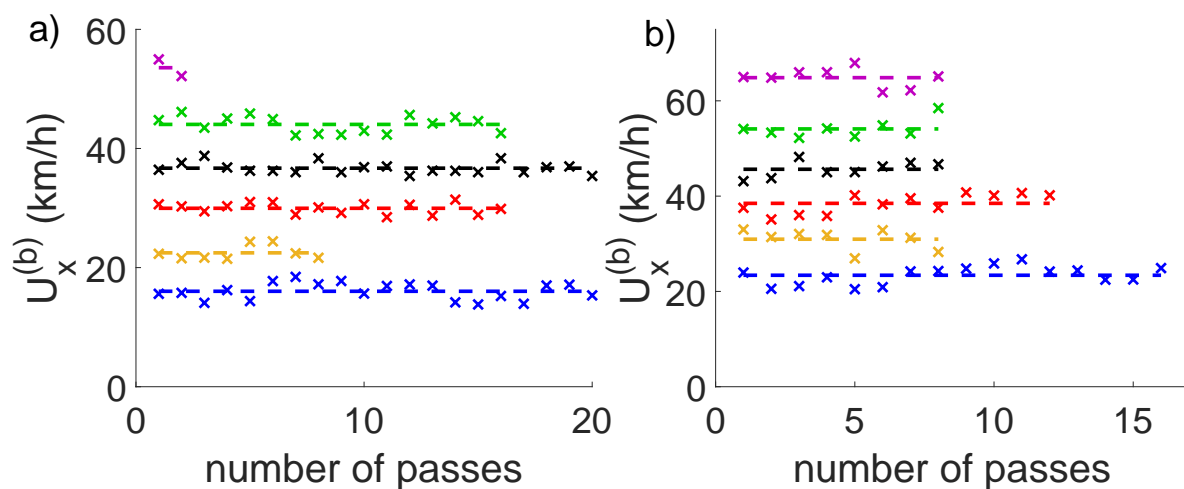


FIGURE 9 – Mean streamwise velocity in the water bank for every passages (crosses) for all vehicle speeds (blue  $V = 30$  km/h, yellow  $V = 40$  km/h, red  $V = 50$  km/h, black  $V = 60$  km/h, green  $V = 70$  km/h and purple  $V = 80$  km/h). Dashed line represent the mean value o the mean velocities for a) New tire, b) Worn tire.

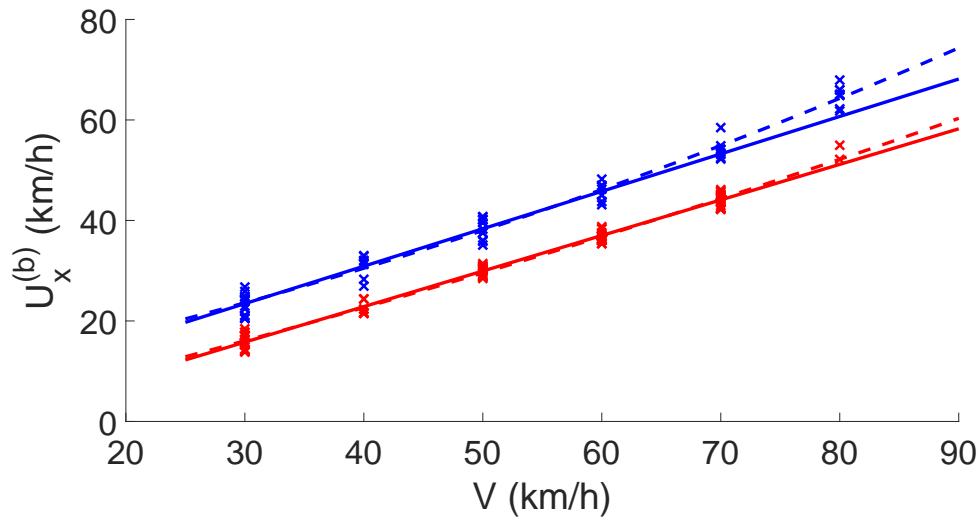


FIGURE 10 –  $U_x^{(b)}$  velocity in the water bank zone depending on the vehicle speed. Blue crosses are the worn tire measurements and the red crosses are the new tire measurements. Solid lines are linear regressions for both cases. Dashed lines are quadratic regression.

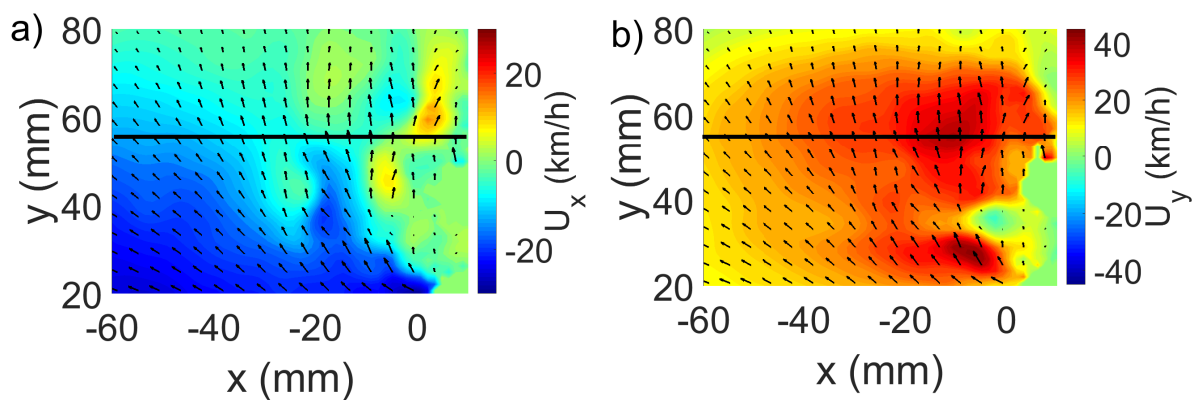


FIGURE 11 – Vector field at the upper shoulder zone of the tire with colormap : a) streamwise velocity ( $U_x$ ), b) spanwise velocity ( $U_y$ ). Black lines define the position of the line along which the velocity  $U_y^{(s)}$  is studied.

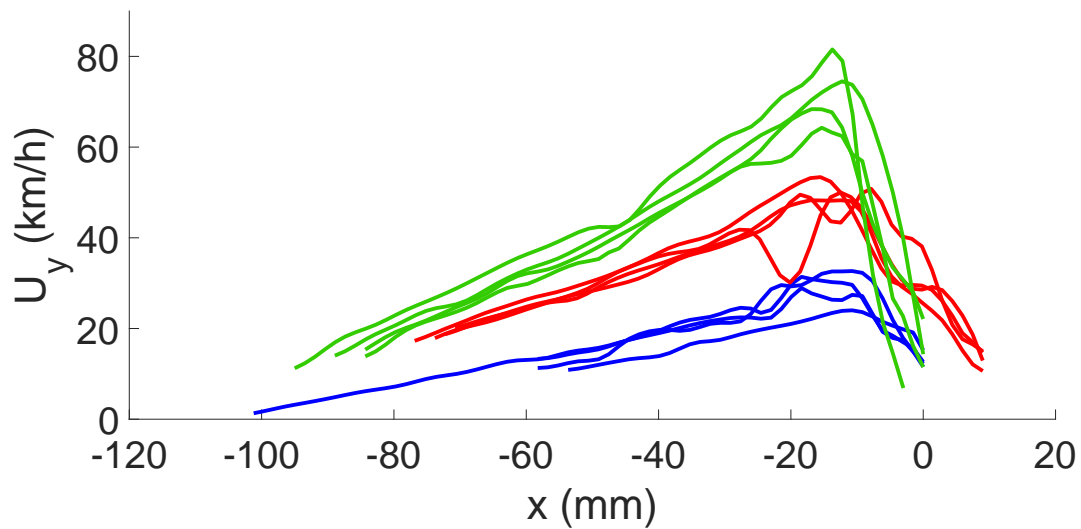


FIGURE 12 – Example of the velocity  $U_y$  obtained along the black line Fig.10 for a measurement night with new tire and  $h_{water} = 8$  mm. Blue lines are the 4 passages at 30 km/h vehicle speed, red lines are 4 passages at 50 km/h and green are the 4 passages at 70 km/h.

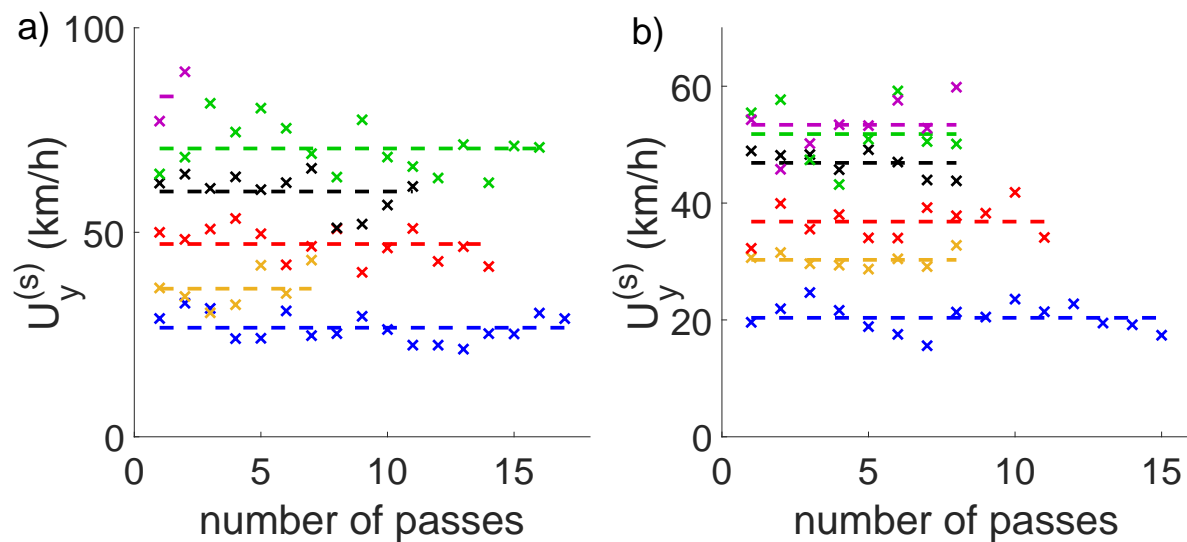


FIGURE 13 – Maximum spanwise velocity at the shoulder for every passages (crosses) for all vehicle speeds (blue  $V = 30$  km/h, yellow  $V = 40$  km/h, red  $V = 50$  km/h, black  $V = 60$  km/h, green  $V = 70$  km/h and purple  $V = 80$  km/h). Dashed line represent the mean value of the maximum velocities for a) New tire, b) Worn tire.

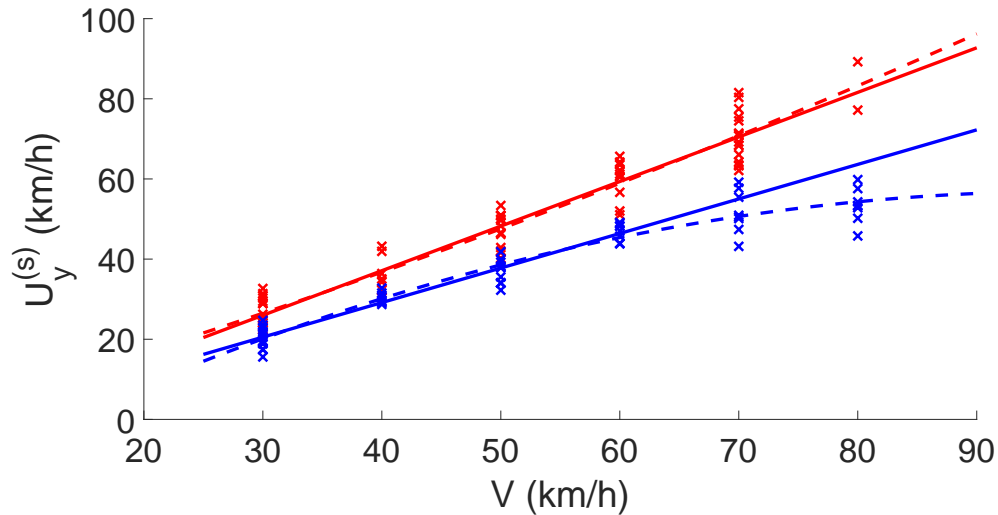


FIGURE 14 –  $U_y^{(s)}$  velocity along the shoulder line for the new tire (red crosses) and the worn tire (blue crosses). Red solid line is the linear regression and red dashed line is the quadratic regression for new tire points. Blue line is the linear regression from  $V = 30$  km/h to  $V = 60$  km/h and blue dashed line is the quadratic regression for the worn tire points.

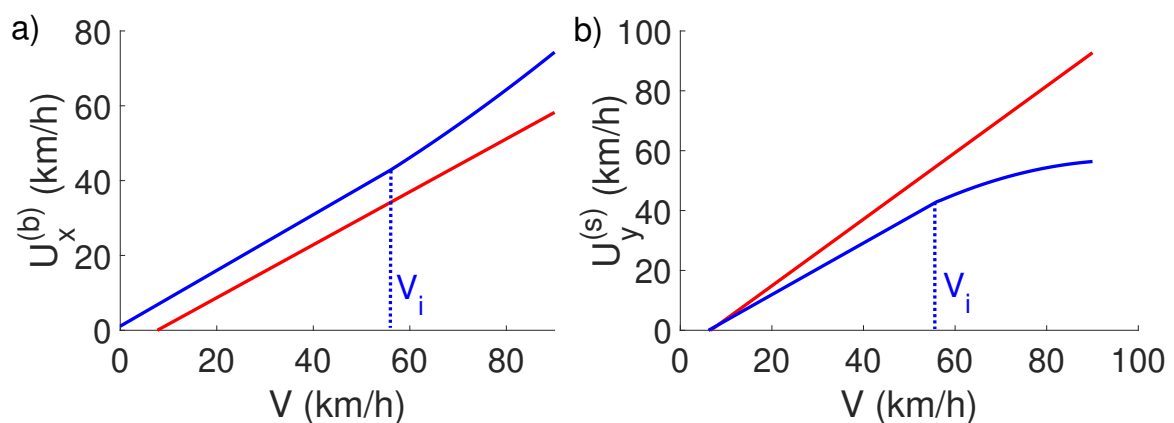


FIGURE 15 – Evolution of  $U_x^{(b)}(V)$  (left) and  $U_y^{(s)}(V)$  (right) for the worn tire in blue and the new tire in red.  $V_i$  represents the inflection speed for the worn tire.